INDICATION FOR THE TEMPORARY PRODUCTION OF DEUTERON-DEUTERON FUSION NEUTRONS DURING ELECTROLYTIC INFUSION OF DEUTERONS INTO A MASSIVE PALLADIUM SLAB

COLD FUSION

TECHNICAL NOTE

KEYWORDS: *d-d* fusion neutrons, electrolytic infusion, loaded palladium

MICHAEL BITTNER, ANDREAS MEISTER, DETLEF OHMS, ELIEF PAFFRATH, DIETMAR RAHNER, RAINER SCHWIERZ, DIETER SEELIGER, KLAUS WIESENER, and PETER WÜSTNER
Technische Universität Dresden, Mommsenstraße 13, O-8027 Dresden, Federal Republic of Germany

Received February 28, 1991
Accepted for Publication May 6, 1991

Two successive long-duration experiments for the observation of deuteron-deuteron (d-d) fusion neutrons emanating from a massive palladium slab are described. The experimental effects observed are discussed through the use of a simple plasmalike model for the time dependence of fusion reactions in condensed matter, which is modified for a plane geometry. This results in a plasma fusion rate of $\lambda_{d\text{-}d}^{Pl} = (1.0 \pm 0.15) \times 10^{-44}\ s^{-1}$. *While plasmalike behavior leading to observable d-d fusion reaction intensities occurs temporarily, under nonequilibrium conditions of electrolytic charging only, for permanently occurring d-d molecular fusion in the fully loaded palladium slab from the experiments, only an upper limit can be set, which is given by* $\Lambda_{d\text{-}d} < 10^{-26}\ s^{-1}$.

I. INTRODUCTION

This technical note continues the presentation of results on the weak neutron production caused by possible deuteron-deuteron (*d-d*) fusion processes in condensed matter carried out at Technische Universität Dresden since April 1989 (Refs. 1 through 5).

The experimental method was described in detail in Ref. 1. Essentially, it consists of the long-term observation of possible *d-d* fusion neutrons emanating from an electrolytic cell containing a massive palladium cathode during electrolytic charging, the deuterons being measured relative to the background as well as relative to other cells using a fast neutron proton-recoil spectrometer. Measurements relative to cells containing light water and others with zero electrolytic current are also included.

For physical discussions of the time structure of possible *d-d* fusion processes in cylindrical geometry, a simple plasmalike model was proposed in Ref. 2; the model is modified here for a plane geometry.

This technical note describes investigations of long-term effects in the massive palladium slab AH1. This cathode was observed during two successive experimental cycle series (ECS) to determine the behavior of the background (an empty position near the detector) and of two other massive but cylindrical electrodes. The behavior of the cylindrical electrodes is presented in Refs. 3 and 4.

II. EXPERIMENT

The ECS2 ran from May 23–June 2, 1989. For 213 h, the two-electrode slab AH1 and the stressed cylinder Stab1 were electrolytically charged, and the corresponding neutron production was observed in a sequence of 1-h measurements relative to the background count rate.

After an ~50-h interruption in the measurements, ECS3 was started; in this experiment, slab AH1, which was without previous discharge, was investigated further in relation to the behavior of the two massive cylinders Z1 and Z2 for ~760 h. ECS3 ran from June 3–July 7, 1989.

The dimensions of the uncharged slab AH1 are 49.8 × 40.3 × 7.1 mm, corresponding to 171.796 g of high-purity palladium. A platinum grid ~5 mm from both sides of the palladium surface was used as the anode. The 3 *M* electrolytic solution of LiOD in D_2O was driven with a constant electric current of $I = 8$ A, corresponding to an electric current density of ~200 $mA \cdot cm^{-2}$. (For simplicity, only the front and back surface areas are taken into account.) The deuterium content was checked by weighing the cathode before and after each experimental cycle. (After ECS3, the weight was determined twice: before and after outgassing in a vacuum stove.) Additionally, each experimental cycle was briefly interrupted once for weighing; otherwise, the electrolysis continued without interruptions. Because of the sampling

procedure of the measurements, the total number of single 1-h measurements for each electrode and background is much less than the entire duration of the experimental cycle. For ECS2, there are 49 and 52 measurements for AH1 and for the empty position in front of the detector, respectively. For ECS3, the numbers are 149 and 162, respectively.

After about every 8 h, the stability of the detector and the energy calibration were checked by using radioactive sources. The pulse-height spectrum or proton-recoil energy (PRE) was recorded both in 512 channels of a multichannel analyzer as well as in the following, more sensitive, broad channel ranges (CHRs).

CHR2: PRE 1.4 to 2.9 MeV ,

CHR3: PRE 1.9 to 2.9 MeV ,

CHR4: PRE 2.9 to 4.1 MeV ,

and

CHR5: PRE 4.1 to 8.0 MeV .

Following the reaction

$$d + d \rightarrow {}^3\mathrm{He} + n + 3.269\ \mathrm{MeV}\ , \qquad (1)$$

the desired effects from single *d-d* reactions are expected in both CHR2 and CHR3. The most sensitive reaction-to-background ratio for *d-d* neutrons is expected for CHR3 because of the smaller background. In the higher CHRs, *d-d* neutrons are not expected to contribute to the count rate unless they are produced in very short hypothetical "neutron bursts."[6] However, counts from alternative nuclear processes assumed by other authors[7] could also occur in these CHRs.

The method used here has the following advantages[1]:

1. comparatively low background count rates in CHR2 and CHR3 because of the n-γ and n-μ discrimination of the detector signals
2. satisfactory *d-d* neutron detection efficiencies of 5 and 3% in CHR2 and CHR3, respectively
3. diminution of the influence both of slow drifts or time-dependent external sources of radiation (e.g., cosmic background) on the results because of the consequently relative procedure of these measurements
4. high sensitivity to small effects as a result of the methods used for data reduction, statistical averaging, and integration, which allow average effects down to 1 to 2 count/h to be detected.

III. MEASUREMENT RESULTS

III.A. Weighing the Deuterium Content

Results of weighing electrode AH1 during the experiment are summarized in Table I. During ECS2, the cathode was loaded with >2 g of deuterium and reached an atomic ratio in PdD_x of $x = 0.615$. By outgassing, the cathode lost 33 mg of deuterium during the ~50-h interruption between the two series. In the following long-term electrolytic charging, the deuterium content increased very slowly and reached $x = 0.698$ after 760 h of charging. However, this number must be understood as the average deuterium density for the entire volume of the electrode. Indeed, the distribution of deuterium in the metal, even after several hundred hours of charging, is not expected to be completely homogeneous as the characteristic diffusion time τ_D for the massive slab used is of the order of

$$\tau_D \simeq \frac{h^2}{D} \simeq 280\ \mathrm{h}\ ,$$

where

$h = 0.71$ cm = thickness of the slab

$D \simeq 5 \times 10^{-7}\ \mathrm{cm^2 \cdot s^{-1}}$ = diffusion coefficient.[8]

This means that near the surface of the slab and far from the border, the local density should be much closer to the maximum loading, or $x \simeq 1$.

TABLE I

Determination of Deuterium Content in Palladium Slab Electrode AH1 During Electrolytic Charging*

Experimental Cycle	Date	m (g)[a]	m_D (g)	x	t (h)	t_{eff} (h)
2	May 22	173.140	0	0	0	0
	May 26	174.264	1.124	0.343	95	95
	May 31	175.156	2.016	0.615	213	213
3	June 3	175.123	1.983	0.605	0	213
	June 23	175.203	2.063	0.629	471	684
	July 5	175.426	2.286	0.698	760	973

*X = atomic ratio in PdD_x.

[a]This includes 1.434 g of the platinum conductor fixed to the cathode.

III.B. Neutron Detection During ECS2

In Fig. 1, the count rates in CHR3 for both the cell with AH1 and for the empty position in front of the detector are

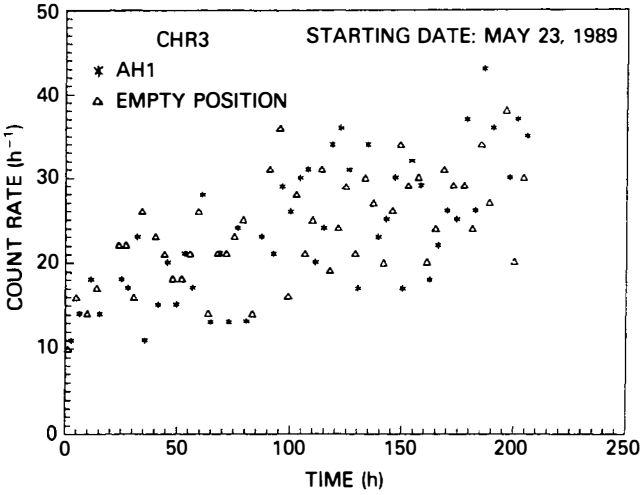

Fig. 1. Experimental count rates for 1-h intervals in CHR3 for the cell with AH1 in front of the detector (noted by asterisks) and the empty position (noted by triangles) during ECS2.

shown. It is already evident that up to the 100-h mark of electrolysis time, the effect counts (marked by asterisks) and background counts (marked by triangles) are at almost the same level, while later on, the effect data are slightly above the corresponding background data. However, this is a very small difference that is scarcely detectable by the eye.

A slow increase in the background level during ECS2 is properly taken into account by the alternating procedure of the measurements.

A rough quantitative idea of the neutron excess observed in the presence of the cell in front of the detector can be obtained from Table II.

The count rate difference (CRD) for the whole experimental cycle is positive, having a confidence level of 2σ. However, in the first half, the CRD is even negative, while in the second half, the difference is definitely positive (with 2.5σ). This behavior can be understood if a "shadow effect" caused by cell AH1 is assumed. This means that an inactive electrolytic cell absorbs a small part of the neutron background from the surroundings, which would otherwise slightly increase the background count rate. This effect was investigated and proved experimentally by additional measurements with massive cylindrical samples both with light water and with cells without electric current.[1] In the present case of the larger cell and the heavier cathode, the effect of background reduction could reasonably be expected within the limits of $-2.0 \pm 1.3\ h^{-1}$ within CHR2 and -1.3 ± 0.9 in CHR3. If this effect is taken into account, the corrected CRDs shown in Table II are obtained. The averaged CRD (ACRD) within 100 h after starting the electrolysis is almost zero (within 1σ); in the second half, it reaches almost 3σ. This is in accordance with the observations for cylindrical cells Z1 and Z2 (Refs. 3 and 4).

If CRDs are averaged over time intervals of 10 or 20 h, a systematic increase in the activity of the electrode can be found, as shown in Fig. 2.

The integrated count rate difference (ICRD), which represents the ACRD from 0 to the variable time t (Ref. 1), is shown for CHR3 and ECS2 in Fig. 3. A slow but continuous increase in the ICRD, starting with negative values and ending with positive is observed as the electrolysis time t increases. Note that in both Figs. 2 and 3, the indicated zero lines still do not take into account the shadow effect. However, both figures show that a reduction of the effective background line by $1.3 \pm 0.9\ h^{-1}$ seems very reasonable because in this case, for the first days of electrolysis, the measured effects are almost exactly equal to zero.

Unfortunately, ECS2 was already finished after 213 h, and so the increase in CRD was not followed up to its maximum.

TABLE II

Averaged Effect (Cell AH1) Minus Background* Count Rate Differences for CHR2 for Different Time Intervals**

Time Interval (h)	Measured Difference (h^{-1})	Corrected Difference (h^{-1})
0 to 100	-2.6 ± 1.5	-0.6 ± 1.9
100 to 213	$+5.0 \pm 2.0$	7.0 ± 2.4
0 to 213	$+2.9 \pm 1.4$	4.9 ± 1.9

*For both empty position measurement and corrected background line.
**During ECS2.

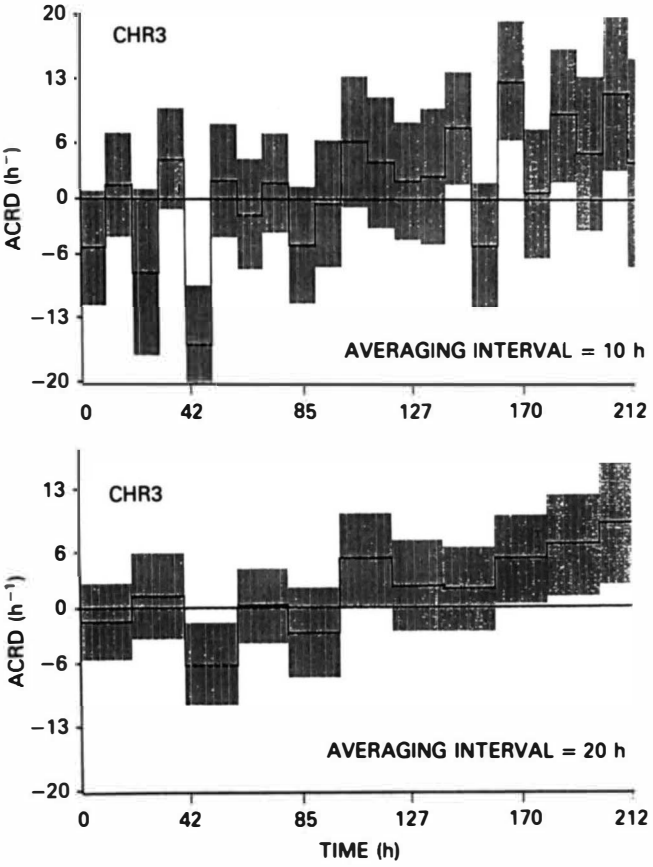

Fig. 2. The ACRDs in CHR3 during ECS2 for averaging intervals of 10 and 20 h.

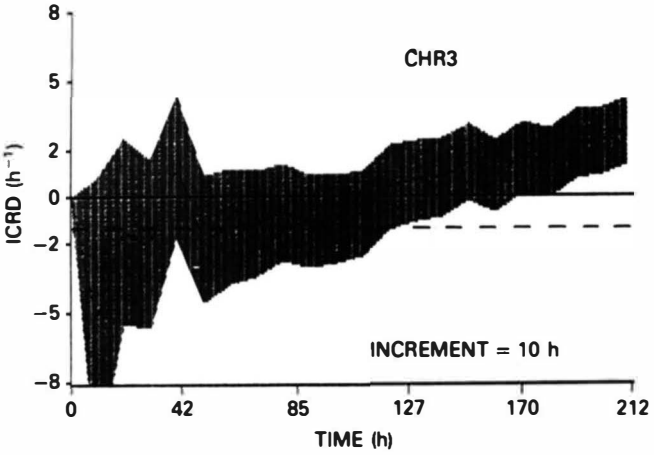

Fig. 3. The ICRDs in CHR3 during ECS2 (1σ corridor) are shown; the dashed horizontal line indicates the corrected background level.

The reason for this was that the first rough data analysis during the experiment was not sensitive enough to recognize the systematic trends of this effect.

Nevertheless, it already became evident at that time that there are some positive effects. Therefore, it was decided to follow the behavior of these effects in comparison with other massive electrodes in ECS3, which started after ~50 h of interruption with no electrolytic current in cell AH1.

III.C. Neutron Detection During ECS3

The ECS3 lasted for 786 h during which cell AH1 ran for 760 h under almost the same electrolytic conditions as in ECS2. Within that 760-h period, cell AH1 was measured 149 times, while the background (empty position) was determined 162 times. Again, each measurement lasted 1 h.

The distribution of background counts in CHR3 and CHR4 as a function of time that is presented in Fig. 4 shows that the spectrometer is reasonably constant. Possible slow shifts of the background level are properly taken into account by the relative procedure of measurements; otherwise, it would be completely impossible to determine CRDs on the order of a few counts per hour.

Tables III and IV present the ACRDs for a few broad time intervals in CHR2 and CHR3, respectively. The corresponding count rate distributions both on an absolute scale and in comparison with a fitted background line are shown in Fig. 5. Both the tables and the figure show that there are positive effects primarily within the first 50 h and in the interval from 205 to 305 h. In the final large interval from 470 to 740 h, the effects are again slightly negative, as at the beginning of ECS2. Obviously, this can be understood as a result of both missing (or rather weak) *d-d* reactions and the shadow effect. The ACRDs in Tables III and IV are obtained after correction for this effect. Within the time interval from 205 to 305 h, both the uncorrected and corrected CRDs are higher than 4σ!

The detailed time structure of the effects can be studied if the CRDs are averaged over successively increasing time intervals, as shown in Fig. 6. This figure confirms the conclusions concerning the most active phases of electrode AH1.

TABLE III

Averaged Effect (Cell AH1) Minus Background* CRD for CHR2 for Different Time Intervals**

Time Interval (h)	Measured CRD (h^{-1})	Corrected CRD (h^{-1})
0 to 45	1.7 ± 1.3	3.7 ± 1.85
45 to 200	0.4 ± 0.6	2.4 ± 1.4
205 to 305	6.0 ± 1.2	8.0 ± 1.8
305 to 470	0.5 ± 0.7	2.5 ± 1.5
470 to 740	−0.7 ± 1.6	1.3 ± 2.1

*For the empty position.
**During ECS3.

TABLE IV

Averaged Effect (Cell AH1) Minus Background* CRD for CHR3 for Different Time Intervals**

Time Interval (h)	Measured CRD (h^{-1})	Corrected CRD (h^{-1})
0 to 45	2.2 ± 0.9	3.5 ± 1.3
45 to 205	0.2 ± 0.35	1.5 ± 1.0
205 to 305	3.5 ± 0.7	4.8 ± 1.1
305 to 470	0.3 ± 0.45	1.6 ± 1.0
470 to 740	−1.8 ± 1.3	−0.5 ± 1.6

*For the empty position.
**During ECS3.

The active phase of AH1 does not coincide with those for the massive cylinders Z1 and Z2, which were measured simultaneously.[3,4] It is also evident that the positive effects are not caused only by single data points, which might be wrong. For

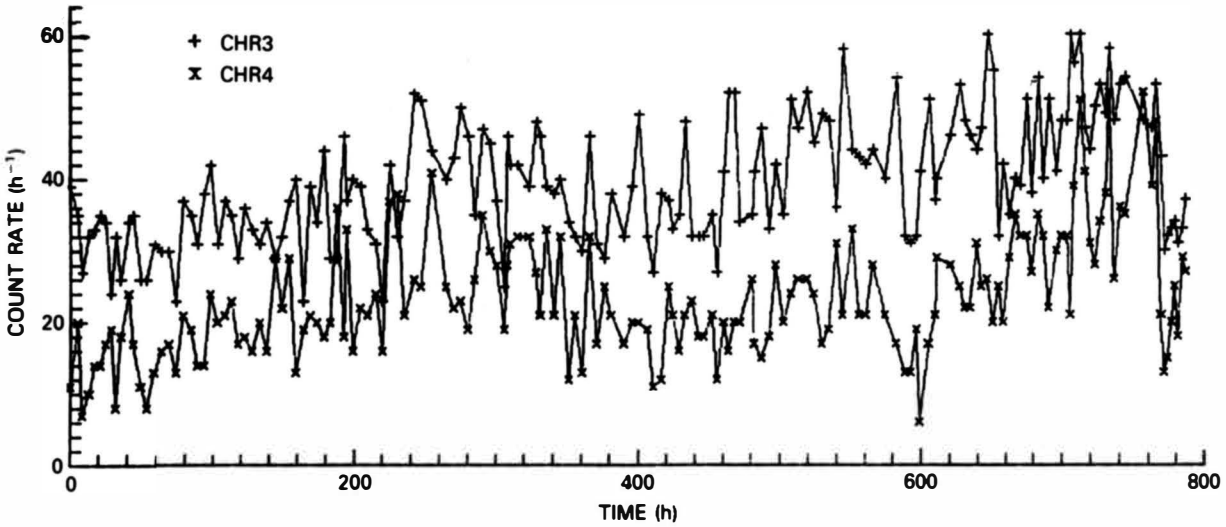

Fig. 4. Experimental background count rates for 1-h intervals in CHR3 and CHR4 during ECS3.

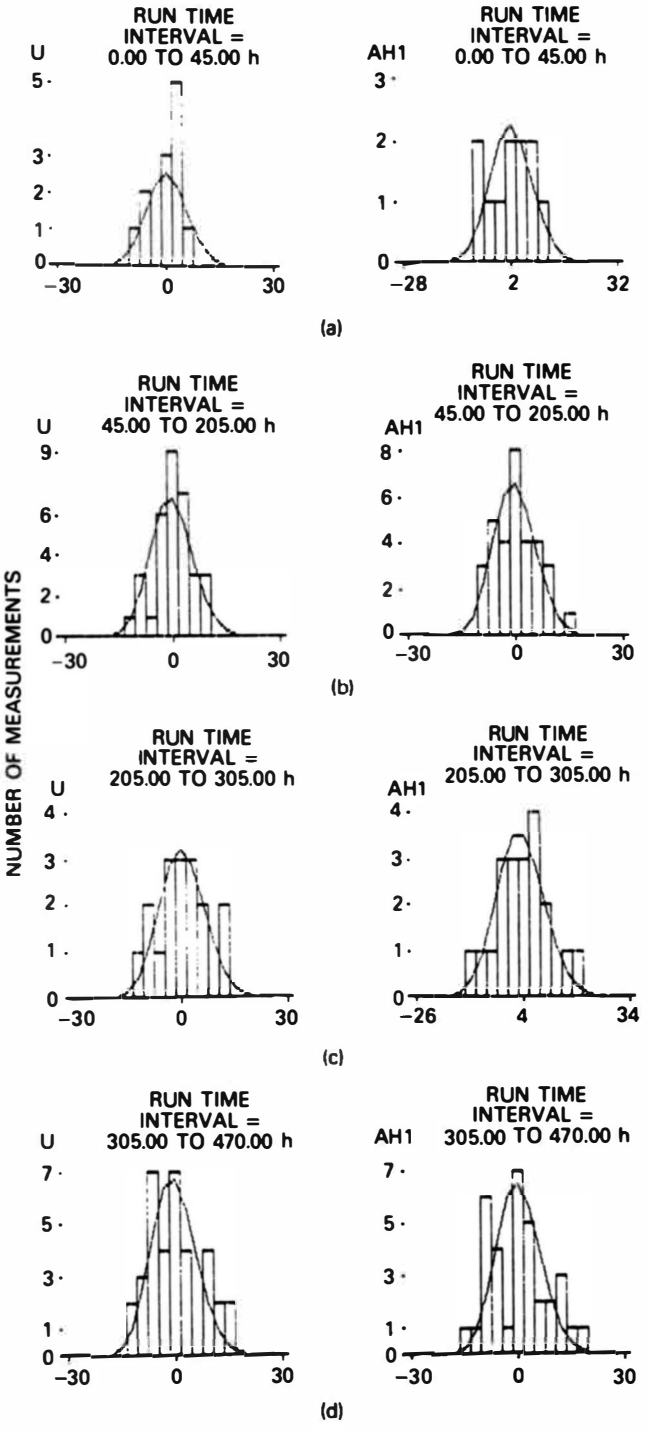

Fig. 5. Distribution of effect and background (empty position) count rates in CHR3 during ECS3 in comparison with Poisson distributions (dotted curves) for different time intervals; the distributions relative to a χ^2 minimum background line obtained from the corresponding uncorrected background data points are shown.

the second half of ECS3, a declining activity in AH1 is characteristic, giving an ACRD within the broad interval from 480 to 760 h in CHR3 of $-1.3 \pm 1.4\ h^{-1}$ as mentioned in Ref. 1.

In Fig. 7, the ACRDs for different CHRs are compared. The different behavior of CHR2 and CHR3 in comparison with CHR4 and CHR5 is evident. Only between 250 to 300 h does there seem to be a small but probably systematic effect in CHR5. However, it is too uncertain for any further physical discussion.

As explained in Ref. 1, a very sensitive tool for recognition of weak but long-term *d-d* fusion reactions is the ICRD, presented in Fig. 8 for the different CHRs of interest. The statistical uncertainty of this value decreases with increasing time and number of measurements. For both CHR4 and CHR5, the ICRD remained zero within 1σ. In both CHR2 and CHR3, it was positive with a confidence level up to 2σ over long time intervals. For $760\ h > t > 470\ h$, where no essential effects were observed, the ICRD decreased. In Figs. 6, 7, and 8, the corrected background levels are not shown.

III.D. Comparisons with Other Cathodes

It is of interest whether or not the positive experimental effects are observed simultaneously for different cathodes utilized in different cells during the same experimental cycle. If they occur simultaneously, it could be suspected that the origin of the effects lies in the same common external sources (e.g., external sources of cosmic radiation) or in a wrong determination of the background level.

Figure 9 compares count rates for CHR3 for slab AH1 with those for the massive cylinder Z2 (which behavior is described in detail in Ref. 4), which started electrolytic loading at $t = 50$ h. Within the interval from 50 to 220 h, the excess count rate from AH1 against Z2, which now is taken as the background level, is of the order of $3\ h^{-1}$. This means that the cell with Z2 in front of the detector does not show effects; its effective count rate is even below that for the empty position (and, in this case, the shadow effect for AH1 is compensated by the background absorption in Z2). Remember that for the similar range shown in Fig. 5b, the excess count rate for AH1 against background (the empty position) was almost zero. Comparison with the numbers in Table IV leads to the conclusion that the correction introduced for the shadow effect is not overestimated but is quite realistic. This figure demonstrates again that in ECS3 cathode AH1 is already active almost from the beginning of the electrolysis, as it was already charged during ECS2.

Figure 10 compares both electrodes within the final, very broad interval from 380 to 740 h. To check the reversibility of this procedure in the upper part, measurements for AH1 are taken as the background, and in the lower part, the data for Z2 are taken as background, giving consistent results in both cases. This figure shows that cathode Z2 was still active for a long time after AH1 had already finished its main activity. Further comparisons between Z2 and another massive cylinder (Z1) are presented in Ref. 4, supporting the conclusion that positive effects observed during the same experimental cycle did not occur simultaneously in different samples. Therefore, the hypothesis that an external source of radiation stimulates the fusion reactions in the metal does not seem realistic. Also, a possibly false determination of the background level as the origin of the observed effects in this way can be excluded from further consideration.

IV. MODEL FOR *d-d* FUSION REACTIONS IN A SLAB CATHODE

In several papers, the occurrence of *d-d* fusion neutrons in metals loaded with deuterium is considered as in a

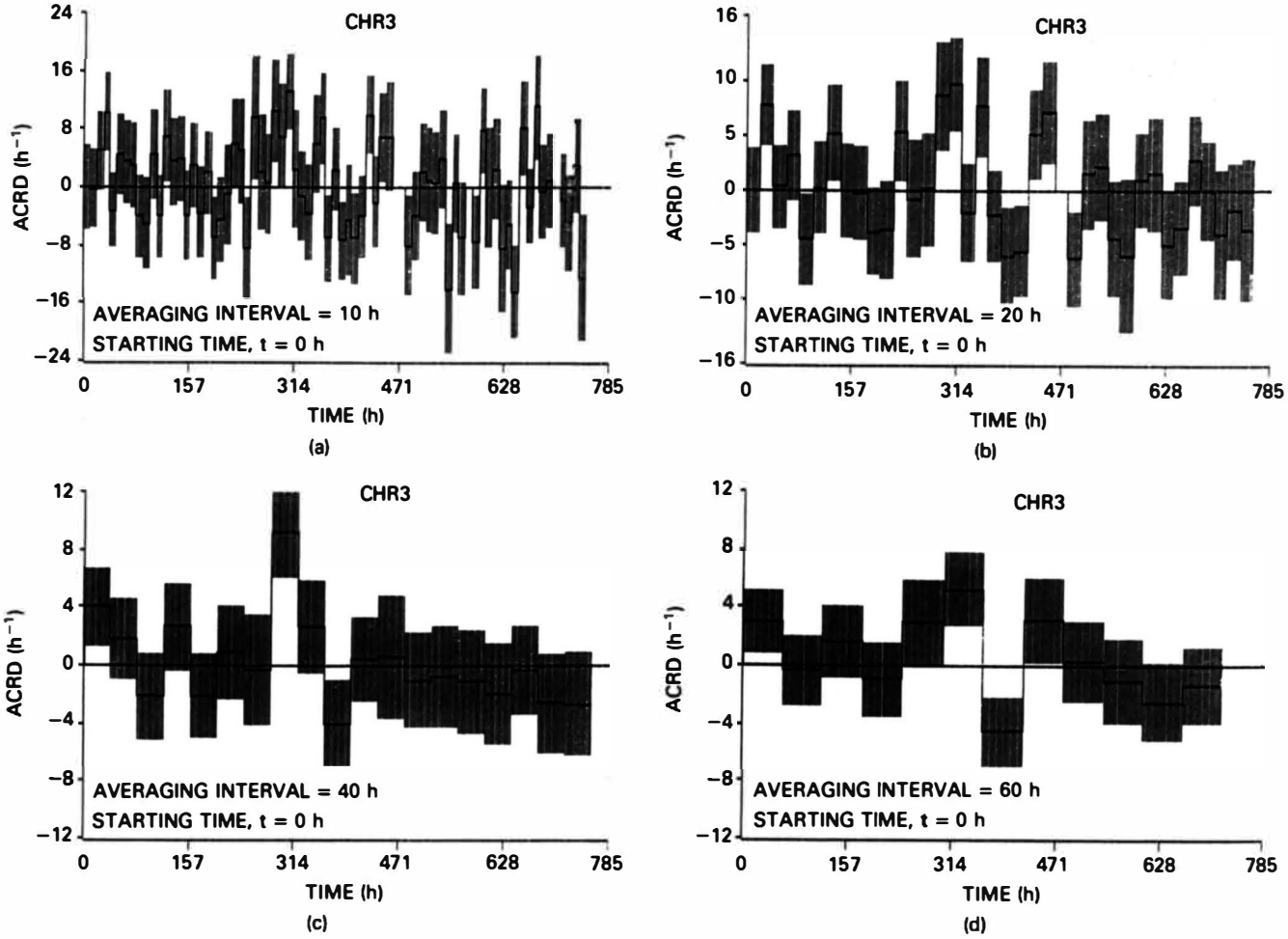

Fig. 6. Average CRDs in CHR3 during ECS3.

D_2 molecular gas where deuterons are fixed together, forming definite *d-d* pairs. For this case, the *d-d* reaction rate $\dot{N}^{d\text{-}d}$ is a linear function of the density n_D, given by

$$\dot{N}^{d\text{-}d}\ (s^{-1}) = \frac{n_D}{2}\,\Delta V \Lambda_{d\text{-}d}\ , \tag{2}$$

where

ΔV = volume of the cathode

$\Lambda_{d\text{-}d}$ = fusion rate per second and deuteron pair.[9]

So far, most of the experiments either have not shown any positive effects at all or, if effects were observed, the resulting fusion rates $\Lambda_{d\text{-}d}$ obtained by Eq. (2) appeared unrealistically high.

An alternative physical description of *d-d* fusion in condensed matter can be provided within a plasmalike description of this process. In this case, it is assumed that deuterons (or a part of them) can move through the metal lattice with velocity v_d and cause collisions with many other deuterons located in the O_h sites of the lattice. The reaction rate in a *d-d* plasma is given by

$$\dot{N}^{d\text{-}d}\ (s^{-1}) = \tfrac{1}{2} n_D^2 \cdot \Delta V \cdot \langle v_d \sigma_{d\text{-}d} \rangle$$
$$= \tfrac{1}{2} N_D \cdot n_D^* \cdot \lambda_{d\text{-}d}^{Pl}\ , \tag{3}$$

where

$\langle v_d \sigma_{d\text{-}d} \rangle\ (cm^3 \cdot s^{-1})$ = product of velocity v_d and reaction cross section $\sigma_{d\text{-}d}$ averaged over the Maxwellian velocity distribution (i.e., plasma reactivity)

n_D^* = dimensionless density number

$N_D = n_D \Delta V \approx$ total number of deuterons within ΔV

$\lambda_{d\text{-}d}^{Pl}\ (s^{-1})$ = plasma fusion rate per deuteron in a flow of particles with unique density $n_D^1 = 1\ cm^{-3}$, moving with a Maxwellian velocity distribution.

A striking difference between the two descriptions is that in the latter case, the reaction rate is proportional to n_D^2 instead of n_D. Therefore, in the plasma, observable effects can

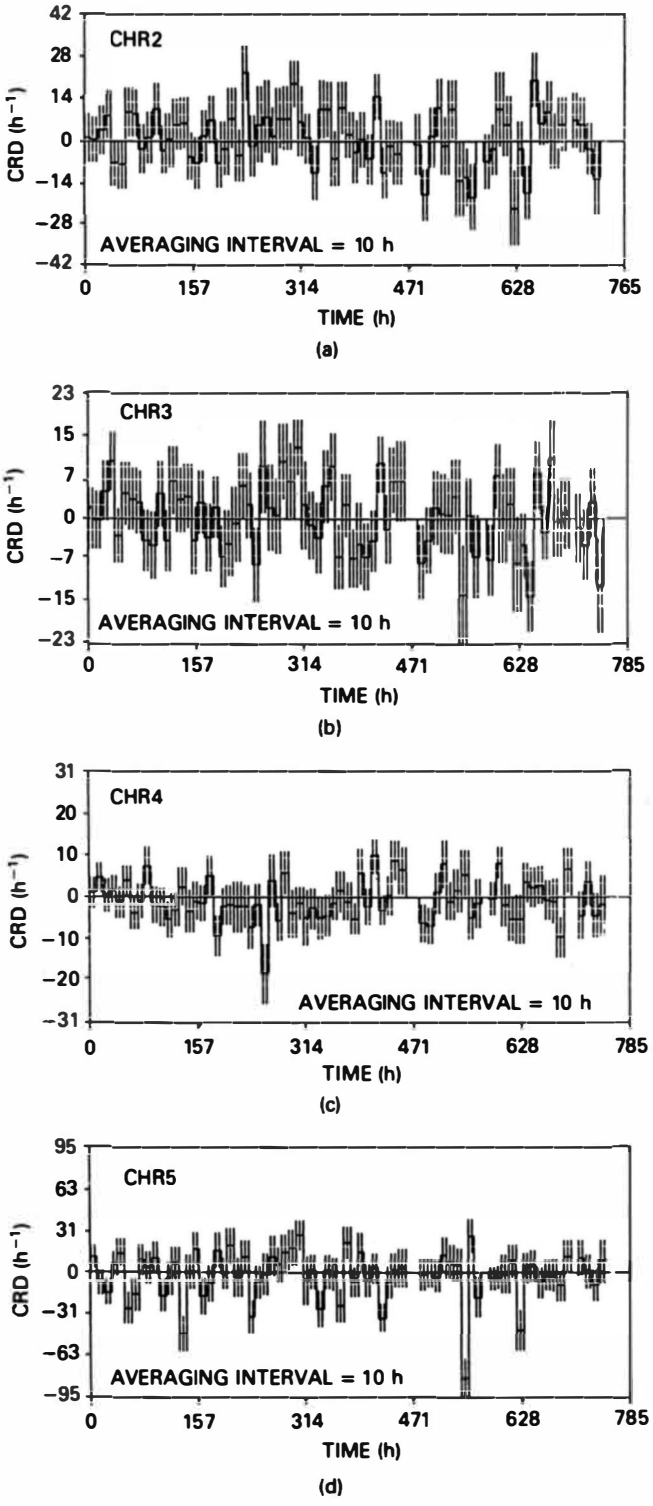

Fig. 7. Average CRDs during ECS3 in CHRs 2, 3, 4, and 5.

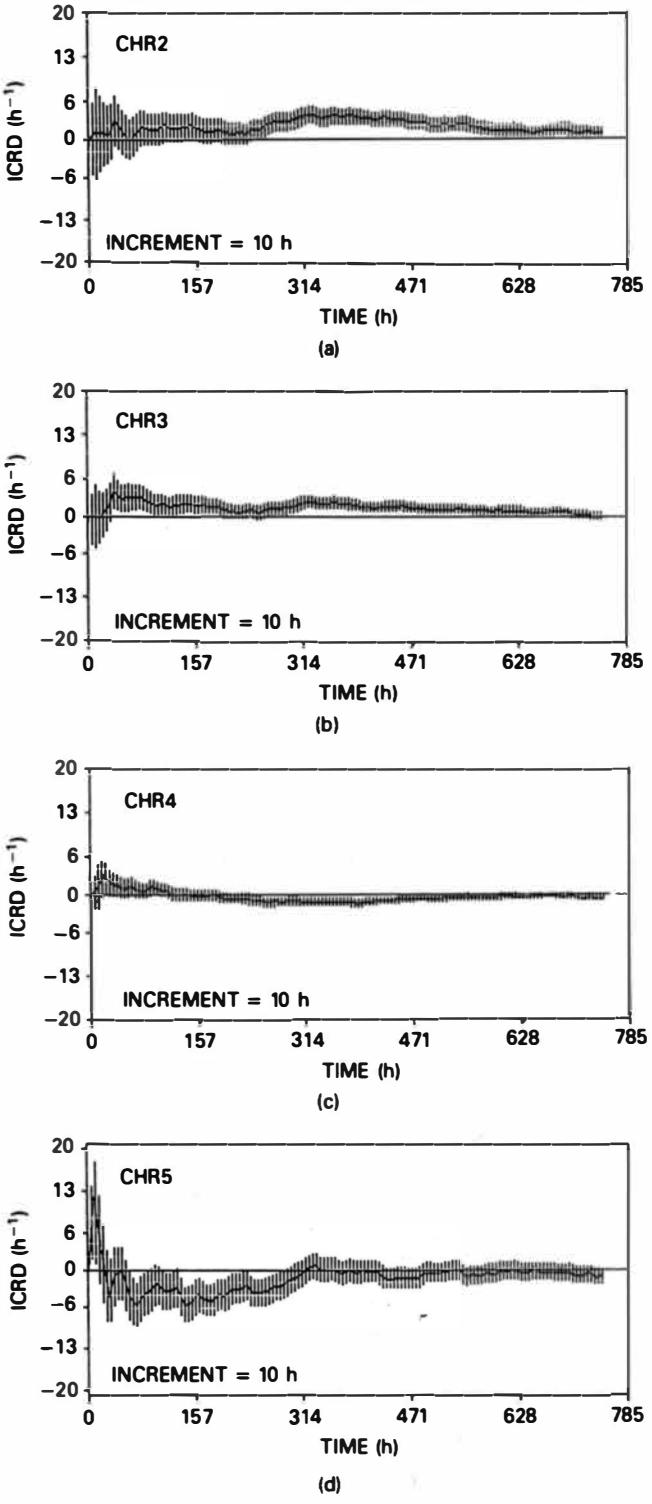

Fig. 8. The ICRDs during ECS3 in CHRs 2, 3, 4, and 5.

be expected for much lower (by many orders of magnitude!) fusion rates than in the case of a behavior seen in D_2 molecules.

Reference 2 presents a simple plasma model for *d-d* fusion processes in a cylindrical sample under nonequilibrium charging conditions. In this model, it was assumed that a part $\kappa[s(t)/s_0]$ of all the deuterons is moving through the metal, causing collisions with other deuterons located in the lattice, which results in a rather small rate of *d-d* reactions:

$$\dot{N}^{d\text{-}d} = n_D^2 \Delta V \kappa \left[\frac{s(t)}{s_0}\right] \lambda_{d\text{-}d}^{PI} , \quad (4)$$

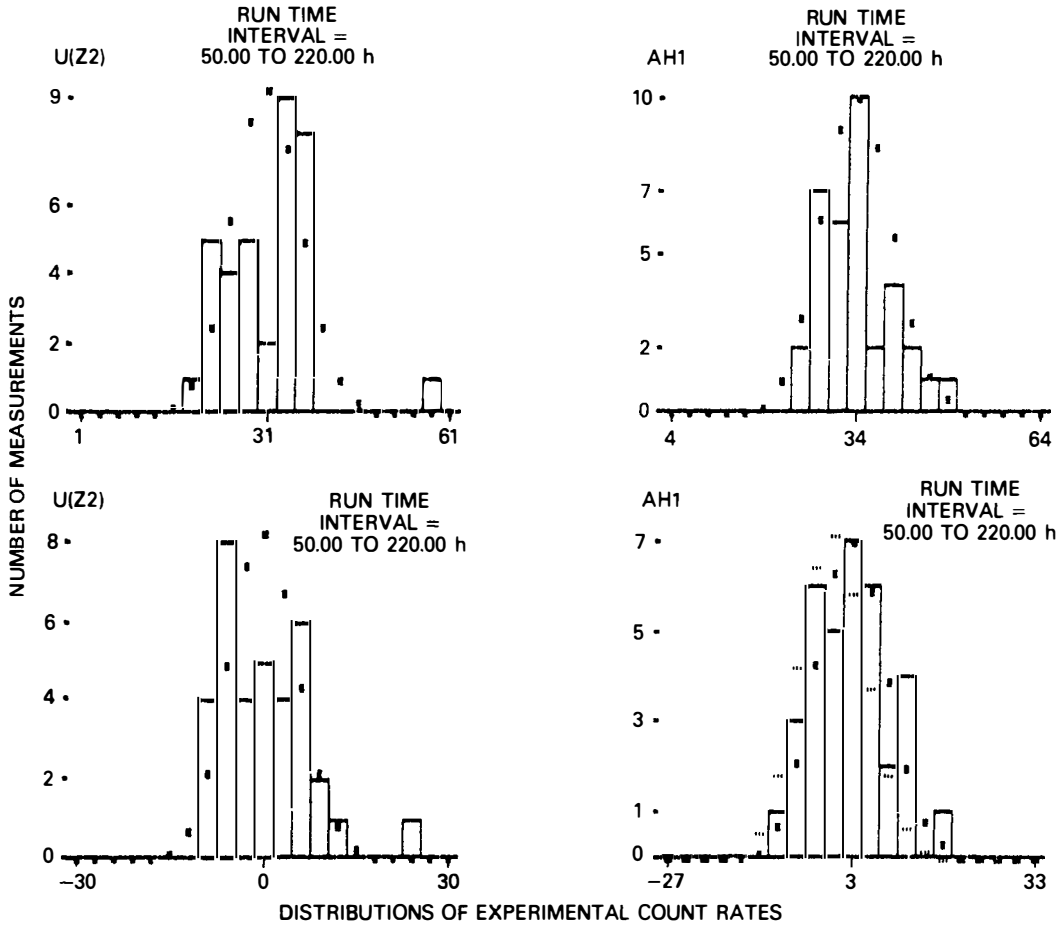

Fig. 9. Distribution of CHR3 count rates for slab AH1 relative to that for cylinder Z2, which is taken as an effective background measurement. The upper part shows absolute count rates, the lower part the distribution relative to a χ^2 minimum background line obtained from the Z2 measurements. Dots represent the shape of corresponding Poisson distributions.

where

$\kappa = \exp\left(-\frac{V_0}{kT}\right)$ = mobile part of deuterons in the metal

$s(t), s_0$ = particle flow density through the surface after time t and at the beginning ($t = 0$)

$V_0 = 0.2\,\text{eV}$ = activation energy for the diffusion of deuterium in palladium

kT = kinetic energy of particles in the plasma at temperature T

k = Boltzmann constant.

The average rate of *d-d* fusion processes depending on time for a cylindric sample was derived in Ref. 2. The corresponding expressions for average reaction rates (ARRs) and integrated reaction rates (IRRs) in a slab-shaped cathode can be formulated easily: The volume of the slab (see Fig. 11) is the product of surface area A (in centimetres squared) and thickness h (in centimetres):

$$\Delta V = Ah \ . \tag{5}$$

For simplicity, first assume a constant loading of the slab through the front and backward surfaces A by a particle flow density s_0 (particles per square centimetre per second). In this case, the average density of deuterons in the metal as a function of time is

$$n_D(t) = \frac{1}{\Delta V}\int_0^t \int_A s_0\, dA\, dt = \frac{2}{h}\, s_0 t \ , \tag{6}$$

resulting in a reaction rate

$$\dot{N}^{d\text{-}d} = \frac{4As_0^2}{h}\, t^2 \kappa \lambda_{d\text{-}d}^{PI} \sim t^2 \ . \tag{7}$$

As for a cylinder, a quadratic dependence of the ARR on t can also be expected for the slab-shaped cathode at moderate loadings as a consequence of the plasmalike ansatz in Eq. (4).

Following the arguments in Ref. 2, at a higher loading, a saturation effect can be expected, which is taken into account by a time-dependent particle flow density:

$$s(t) = s_0\left[1 - \frac{n_D(t)}{n_D^{max}}\right] < s_0 \ , \tag{8}$$

where n_D^{max} is the maximum deuteron density achievable in the metal.

Instead of the relationship in Eq. (6), the relation between $s(t)$ and $n_D(t)$ is now given by the differential equation

$$\frac{dn_D(t)}{dt} = \frac{2}{h}\, s(t) \ . \tag{9}$$

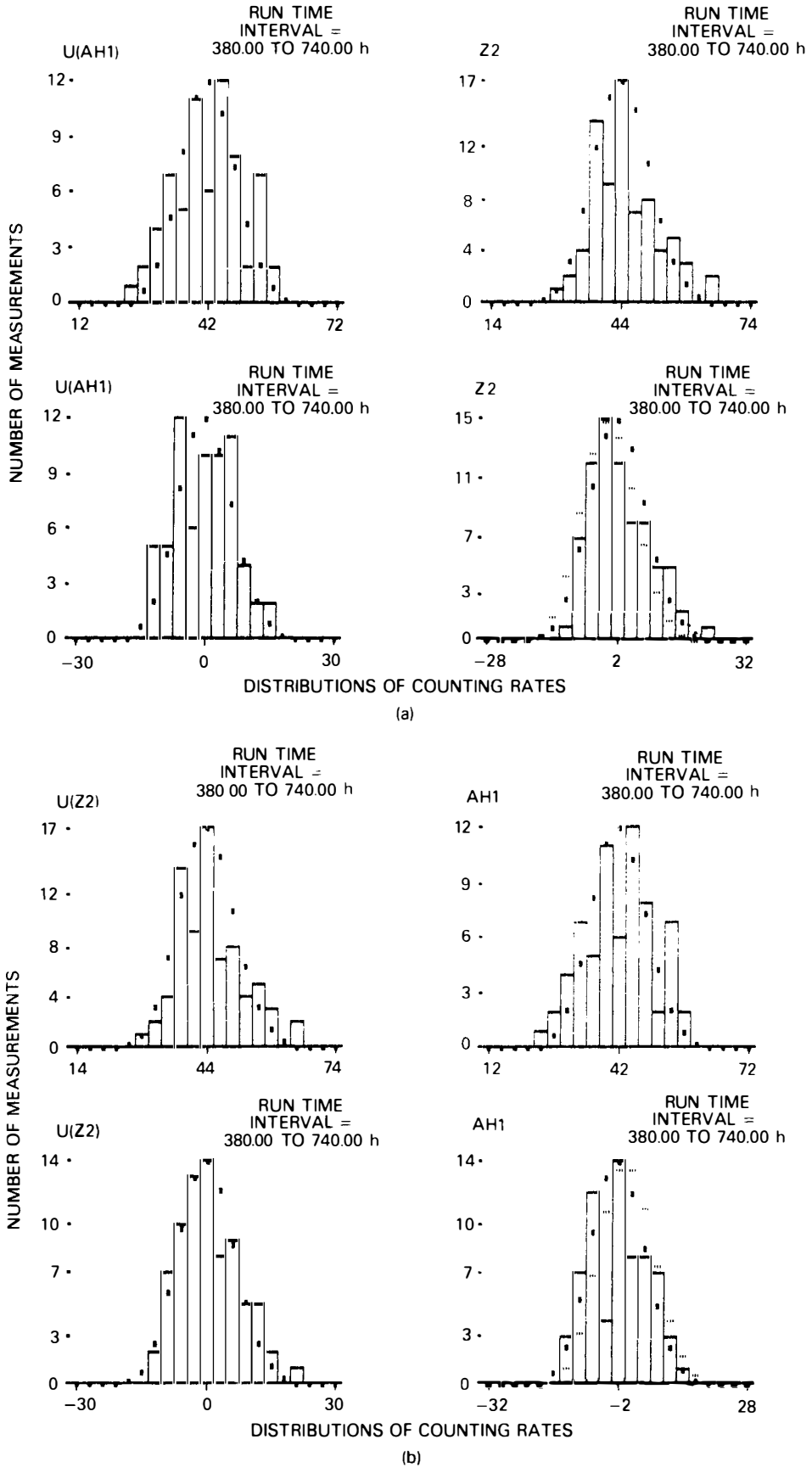

Fig. 10. Distribution of CHR3 count rates for slab AH1 relative to cylinder Z2 for a run time interval of 380 to 740 h; in this case, the measurements with AH1 are compared with Z2 background (upper part), and vice versa (lower part), giving consistent results.

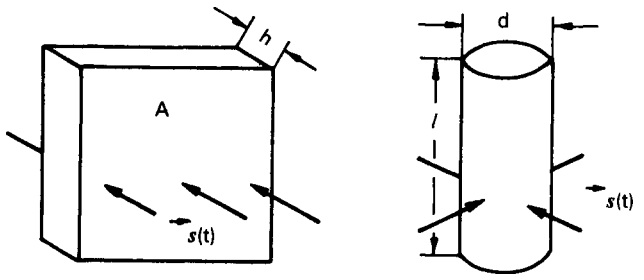

Fig. 11. Charging of palladium cathodes in slab and cylinder geometry.

From Eqs. (8) and (9), the solutions

$$n_D(t) = n_D^{max}\left[1 - \exp\left(-\frac{2s_0}{hn_D^{max}}\,t\right)\right] \tag{10}$$

and

$$s(t) = s_0 \exp\left(-\frac{2s_0}{hn_D^{max}}\,t\right) \tag{11}$$

are obtained.

The reaction rate now becomes

$$\dot{N}^{d\text{-}d} = (n_D^{max})^2 Ah\left[1 - \exp\left(-\frac{t}{t_L}\right)\right]^2 \exp\left(-\frac{t}{t_L}\right)\kappa\lambda_{d\text{-}d}^{Pl}\ , \tag{12}$$

with the loading time constant

$$t_L = \frac{hn_D^{max}}{2s_0}\ . \tag{13}$$

Equation (13) again predicts a broad maximum of $\dot{N}^{d\text{-}d}$ near $t = t_L$, i.e., at 63% of the full loading of the electrode. The IRR $\langle \dot{N}^{d\text{-}d} \rangle$ now amounts to

$$\begin{aligned}\langle \dot{N}^{d\text{-}d} \rangle &\equiv \frac{1}{t}\int_0^t \dot{N}^{d\text{-}d}\,dt \\ &= (n_D^{max})^2 Ah\,\frac{t_L}{t}\left\{\frac{1}{3} - \exp\left(-\frac{t}{t_L}\right)\left[1 - \exp\left(-\frac{t}{t_L}\right) + \frac{1}{3}\exp\left(-\frac{2t}{t_L}\right)\right]\right\}\kappa\lambda_{d\text{-}d}^{Pl} \\ &\sim \frac{1}{x}\left\{\frac{1}{3} - \exp(-x)\left[1 - \exp(-x) + \frac{1}{3}\exp(-2x)\right]\right\},\end{aligned} \tag{14}$$

with $x = t/t_L$.

Neglecting boundary effects (i.e., particle flow through the outer surface) for cylindrical and slab-shaped electrodes having the same volume, the reaction rates are expected at the same level and with similar time dependence. However, there is a difference in the corresponding loading time constants:

slab:

$$t_L = \frac{hn_D^{max}}{2s_0} \tag{13}$$

cylinder:

$$t_L = \frac{dn_D^{max}}{4s_0}\ , \tag{15}$$

where d is the diameter of the cylinder.

Finally, the cumulative effect $N_\Sigma^{d\text{-}d}(t)$, i.e., the total number of reactions up to a given time t, reads

$$\begin{aligned}N_\Sigma^{d\text{-}d}(t) &\equiv \int_0^t \dot{N}_\Sigma^{d\text{-}d}(t) \\ &= (n_D^{max})^3\,\frac{Ah^2}{2s_0}\left\{\frac{1}{3} - \exp(-x)\left[1 - \exp(-x) + \frac{1}{3}\exp(-2x)\right]\right\}\kappa\lambda_{d\text{-}d}^{Pl}\ ,\end{aligned} \tag{16a}$$

and the total cumulative effect up to $t = \infty$ amounts to

$$N_\Sigma^{d\text{-}d}(\infty) = (n_D^{max})^3\,\frac{Ah^2}{6s_0}\,\kappa\lambda_{d\text{-}d}^{Pl} = \frac{1}{3}\,(n_D^{max})^2 \Delta V t_L\,\kappa\lambda_{d\text{-}d}^{Pl}\ . \tag{16b}$$

The cumulative number of reaction events for cathodes of the same volume ΔV is proportional to t_L, giving a relation of

$$\frac{\text{cumulative effect slab}}{\text{cumulative effect cylinder}} = \frac{2h}{d}\ (\text{for } \Delta V = \text{constant})\ , \tag{17}$$

if it is assumed that s_0 and n_D^{max} are the same for both cases. If ΔV is not constant, the corresponding relation amounts to

$$\frac{\text{cumulative effect slab}}{\text{cumulative effect cylinder}} = \frac{8}{\pi}\,\frac{Ah^2}{ld^3}\ , \tag{18}$$

where l is the length of the cylinder.

V. MODEL PARAMETERS

For application, several parameters of the model must be fixed: n_D^{max}, s_0, and κ.

The part of mobile deuterons can be obtained easily by taking a typical activation energy of $V_0 = 0.2$ eV (Ref. 8) and a temperature $T = 320$ K, resulting in $\kappa = 7.08 \times 10^{-4}$.

The maximum loading of palladium is usually chosen to be PdD_x, with $x = 1.0$, resulting in $n_D^{max}(x = 1) = 6.8 \times 10^{22}$ cm^{-3}. However, the weighing of cathode AH1 during the course of our experiment (see Table I) resulted in a somewhat lower maximum content, corresponding only to $x \simeq 0.7$.

There might be two reasons for this difference: First, the outer surface of slab AH1 is of the order of 32% compared with surface area 2A through which the loading takes place. This might lead to permanent losses of some deuterium from the part of the volume near the border during the electrolysis. Second, the characteristic diffusion time $\tau_D \simeq 280$ h is not small in comparison with the duration of the experiment. Therefore, inside the volume ΔV there remains a finite gradient of the density n_D. For both reasons, we conclude that in the central area near surfaces A, the deuteron density is much closer to $x = 1$ than is deduced from weighing. Therefore, for model applications, the maximum density is fixed at $n_D^{max} = 6.8 \times 10^{22}$ cm^{-3}, as for the cylindrical samples Z1 and Z2 (Refs. 3 and 4).

The magnitude of particle flow s_0 can be fixed in three ways:

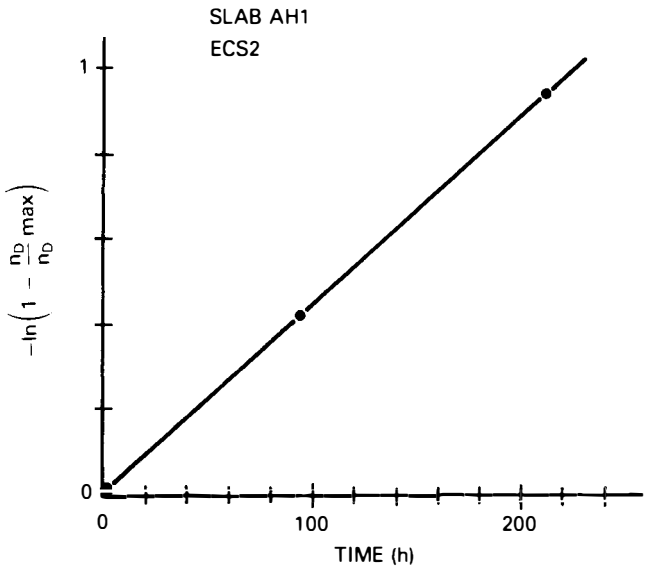

Fig. 12. Charging cathode AH1 with deuterium during ECS2; points are obtained from measured weights of deuterium content in AH1 (see Table I).

1. Comparing the weight measurements of the electrode with results from Eq. (10), the loading time constant t_L that depends both on n_D^{max} and s_0 can be determined. Figure 12 shows the function $\ln[1 - n_D(t)/n_D^{max}]$ versus time for ECS2, the slope of which corresponds to $t_L \simeq 223$ h.

2. The second way is based on the position of the maximum of the observed ACRD, which is expected to be $\sim t \simeq t_L$. This method was used successfully for the interpretation of results for cylindrical electrodes.[3,4] In the current case, this method is somewhat arbitrary, as the electrolysis was interrupted between ECS2 and ECS3, i.e., after 213 h. However, the observed behavior of the ACRD during ECS2 does not contradict the assumption that the maximum ACRD would have been reached at 220 to 230 h if the electrolysis would have been continued.

3. The third way would be to calculate t_L from Eq. (13) using the particle flow density $s_0 = 3.12 \times 10^{16}$ cm$^{-2}\cdot$s^{-1}, corresponding to 5 mA$\cdot$cm^{-2}, which was found useful for the interpretation of Z1 and Z2 (Refs. 3 and 4). This generates $t_L \simeq 215$ h, which is somewhat less, but this might be the result of neglecting the particles lost through the border surfaces during electrolysis.

Therefore, we take $t_L = 223$ h for the theoretical analyses.

VI. DISCUSSION

In Refs. 3 and 4, it was shown that the *d-d* fusion reaction in the massive cylinders Z1 and Z2 is reasonably described by the plasmalike model.[2] It is also of interest if the behavior of slab AH1 can be interpreted in terms of this model.

Figure 13 presents the experimental ARRs for CHR3 in ECS2 and $\Delta t = 20$ h (compare Fig. 2), taking into account both the detector efficiency and the shadow effect. They are compared with the calculations using Eqs. (7) and (12) and the parameters selected as described in Sec. V, adjusting the absolute height of the theoretical curves to the experiment. The absolute adjustment is given with $\dot{N}^{d\text{-}d}(t)/t^2 = (1.6 \pm 0.2) \times 10^{-2}$ h^{-3} and $\dot{N}^{d\text{-}d}(t = t_L) = 300 \pm 30$ h^{-1} for Eqs. (7) and (12), respectively. From Fig. 12, it is evident that Eq. (7) deviates considerably from the experiment for $t > 120$ h. Compared to this, Eq. (12) fits the experiment much better—the calculated curve crosses all the 1σ error bars except one. From the absolute adjustment of Eq. (12), a *d-d* fusion rate of

$$(\lambda_{d\text{-}d}^{Pl})^i = (1.03 \pm 0.10) \times 10^{-44}\ \text{s}^{-1}$$

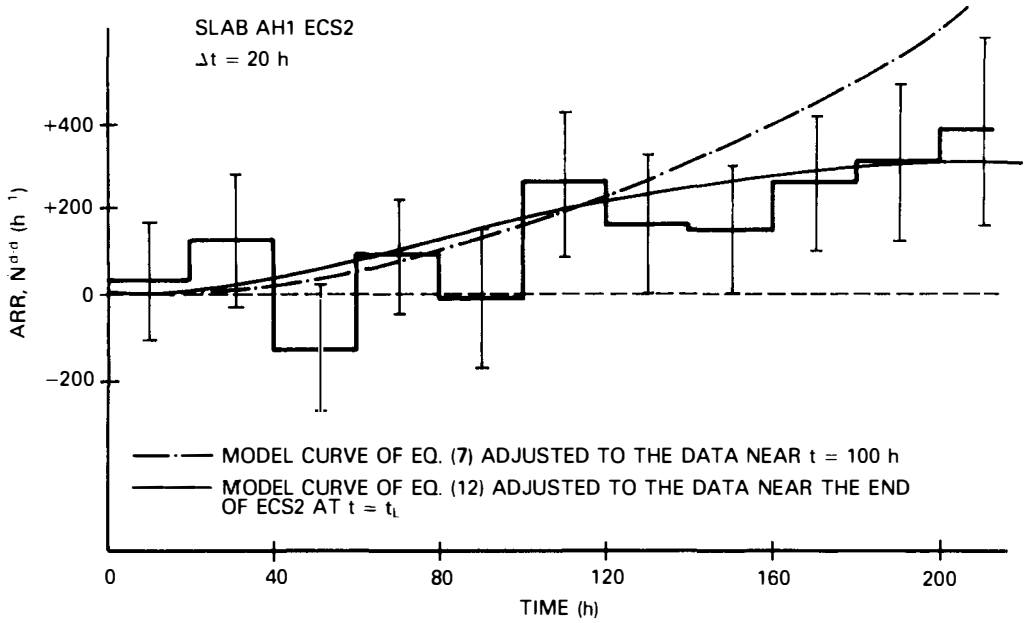

Fig. 13. Average reaction rate $\dot{N}^{d\text{-}d}$ for CHR3 during ECS2; a histogram shows experimental data averaged over 20 h. In this presentation, both the corrected background level and the neutron registration efficiency are taken into account.

is obtained. Using the adjustment of Eq. (7), the plasma fusion rate amounts to

$$(\lambda_{d\text{-}d}^{Pl})^{ii} = (0.67 \pm 0.08) \times 10^{-44}\ \mathrm{s}^{-1} \ .$$

There is less confidence in this value, however, than in the first one: $(\lambda_{d\text{-}d}^{Pl})^{ii}$ could be closer to $(\lambda_{d\text{-}d}^{Pl})^{i}$ if, in the starting phase, the model curve of Eq. (7) would be adjusted higher, i.e., closer to the model curve in Eq. (12). In this case, however, the discrepancies between Eq. (7) and the experiment would become much larger near the end of ECS2. It can be concluded that Eq. (7) is useful as a crude estimate only at very low loadings where $x \lesssim 0.3$.

Another comparison can be provided for the IRRs as given by Eq. (14). The experimental IRRs obtained from ICRDs (see Fig. 3), taking into account both the detector efficiency and the shadow effect, are shown in Fig. 14 in comparison with the model calculation. Both agree well within the 1σ uncertainty corridor. From the absolute calibration, $\langle \dot{N}^{d\text{-}d}(t = t_L) \rangle = 185 \pm 15\ \mathrm{h}^{-1}$ by comparing with Eq. (14), the plasma fusion rate

$$(\lambda_{d\text{-}d}^{Pl})^{iii} = (1.11 \pm 0.09) \times 10^{-44}\ \mathrm{s}^{-1}$$

is derived in agreement with the results for $(\lambda_{d\text{-}d}^{Pl})^{i}$. Combining these two results for $(\lambda_{d\text{-}d}^{Pl})^{i}$ and $(\lambda_{d\text{-}d}^{Pl})^{iii}$, we get the following plasma fusion rate for slab AH1 in ECS2:

$$(\lambda_{d\text{-}d}^{Pl})^{\mathrm{ECS2}} = (1.07 \pm 0.09) \times 10^{-44}\ \mathrm{s}^{-1} \ .$$

The interpretation of results for ECS3 within the plasma model is more difficult, as slab AH1 was already partially charged before the beginning of the measurements. During the interruption between ECS2 and ECS3, the deuterium density distribution within the metal changed by partial outgassing and diffusion compared to the distribution by the end of ECS2. Finally, the conditions at the surface of the cathode might also have been changed slightly during the interruption because the electrode was out of the electrolyte part of the time.

The comparison with the model curve given by Eq. (12) as shown in Fig. 15 does not give satisfactory agreement either for $t_L = 223$ h or for $t_L = 350$ h; the latter loading time constant was used successfully for cylinders Z1 and Z2 (Refs. 3 and 4). However, a better agreement is obtained if ECS2 and ECS3 are combined, as shown in Fig. 16. In this presentation, the time scale for ECS3 starts immediately after the end of ECS2, and the interruption of electrolytic current is omitted. In this case, most of the data points within the 1σ error bars agree with the theoretical curve by Eq. (12) using $t_L = 223$ h. In particular, the activities of slab AH1 in the starting phase of ECS3 are reproduced. However, there is a peak near $t_{(3)} \simeq 300$ h that cannot be reproduced within the model used. It is uncertain whether this could be interpreted as the result of a different mechanism for the *d-d* reactions. [When the electrode was taken out of the cell for weighing after $t_{(3)} \simeq 470$ h, it showed deep cracks, and at the end of ECS3, the thickness of cathode AH1 was increased up to 0.84 cm!] In comparison with Fig. 13, the curve following Eq. (12) was adjusted somewhat lower, giving a *d-d* fusion rate of

$$(\lambda_{d\text{-}d}^{Pl})^{4i} = (0.8 \pm 0.2) \times 10^{-44}\ \mathrm{s}^{-1} \ .$$

It should be stressed, however, that a combined treatment of the ECS2 and ECS3 measurements within the model using a unique time scale is somewhat arbitrary.

A reasonable average over the different values obtained for ECS2 and ECS3 [excepting $(\lambda_{d\text{-}d}^{Pl})^{ii}$] is

$$\lambda_{d\text{-}d}^{Pl} = (1.0 \pm 0.15) \times 10^{-44}\ \mathrm{s}^{-1} \ .$$

There are two possibilities for the determination of the cumulative number of *d-d* reactions:

1. This value can be determined directly from the experiment by summing up the ARRs for $\Delta t = 40$-h intervals shown in Fig. 16 for ECS2 and ECS3. This procedure results in

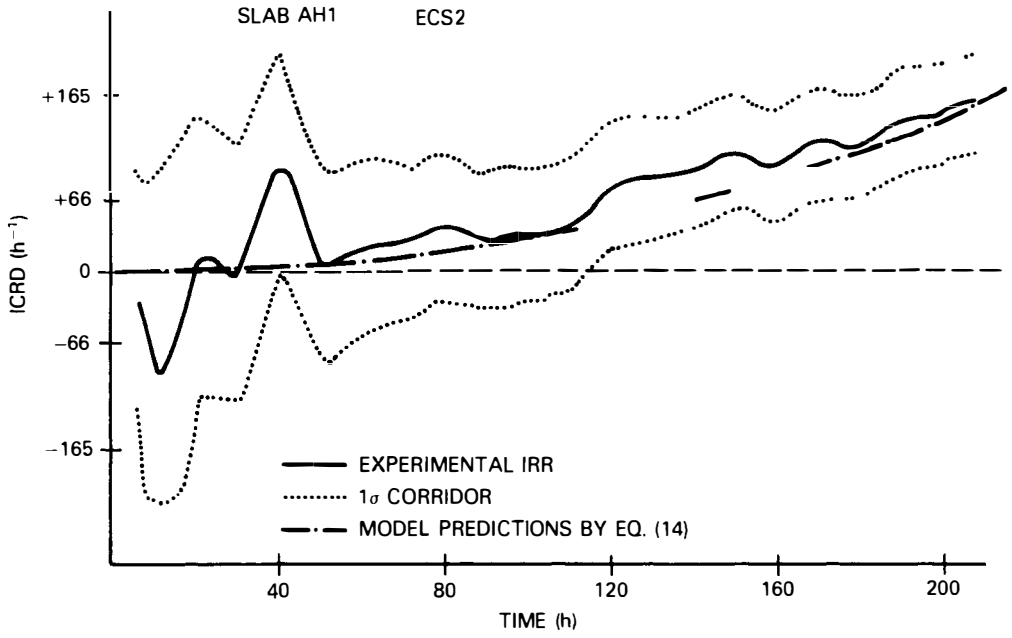

Fig. 14. Comparison between the experimental IRRs for CHR3 during ECS2.

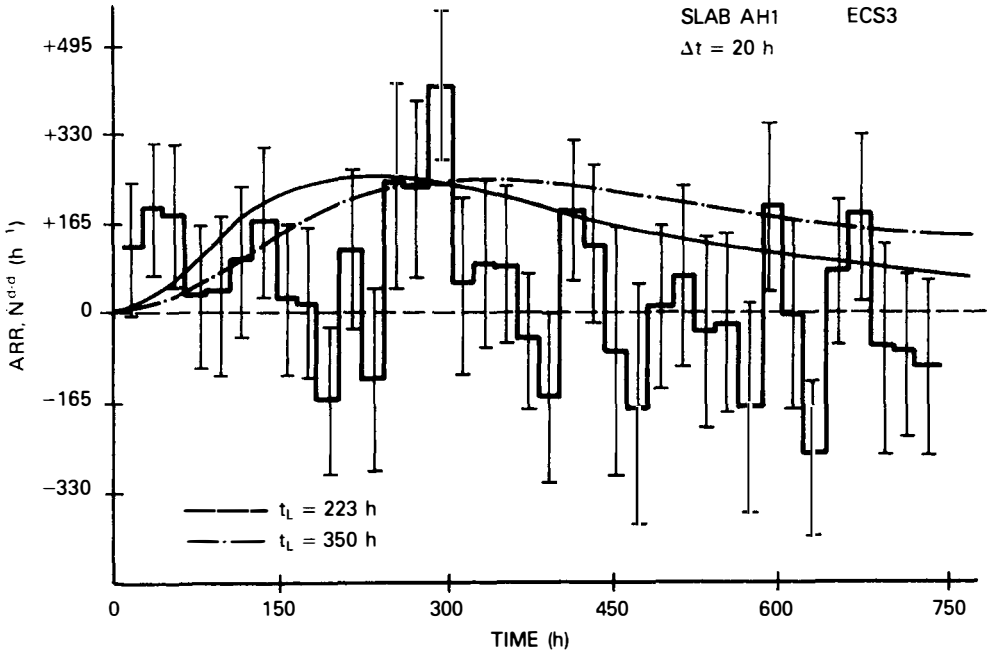

Fig. 15. Average reaction rate $\dot{N}^{d-d}$ for CHR3 during ECS3; model predictions following Eq. (12) are presented.

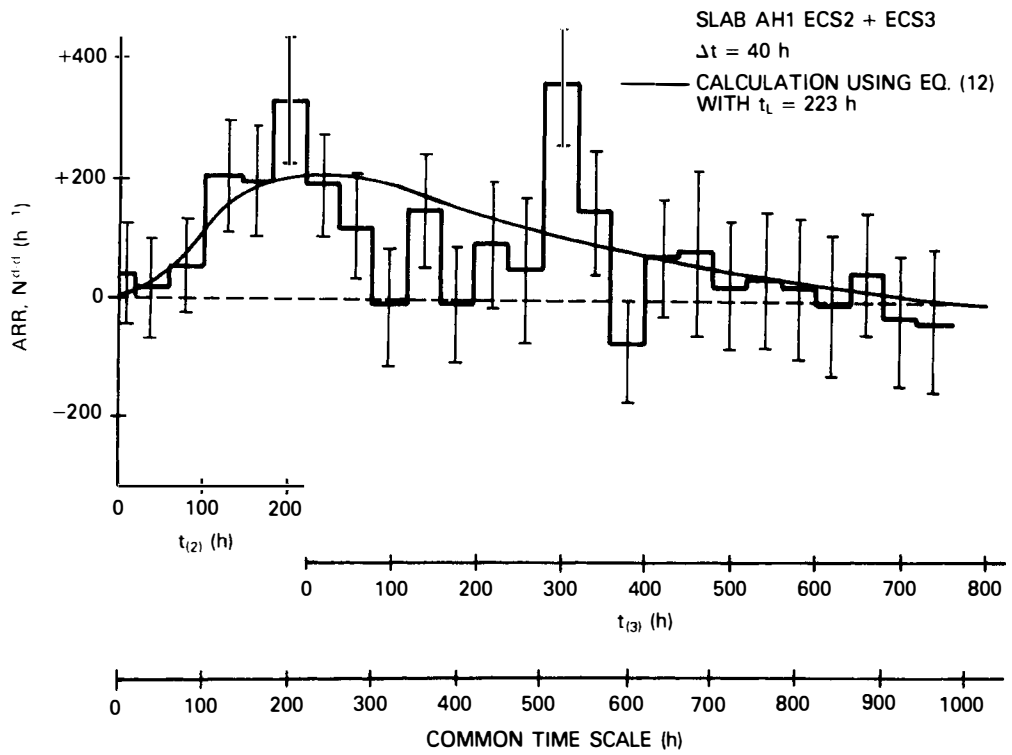

Fig. 16. Average reaction rate $\dot{N}^{d-d}$ for CHR3; the time scales for ECS2 [indicated as $t_{(2)}$] and for ECS3 [indicated as $t_{(3)}$] are combined to a common time scale.

$$N^{d-d}_{\Sigma\text{exp}}(960\text{ h}) = (8.3 \pm 0.6) \times 10^4$$

d-d reaction events in >960 h of electrolysis; this is equivalent to $4.3t_L$.

2. Using the just-determined λ^{Pl}_{d-d} (by adjustment to the experiment near $t \simeq t_L$) along with Eq. (16b), a theoretical number

$$N^{d-d}_{\Sigma,th}(\infty) = (12.5 \pm 1.9) \times 10^4$$

can be derived. The latter is somewhat higher than the first one, as in the second half of ECS3 the experimental reaction rates decrease faster than the model curve (cf. Fig. 16). Having in mind that our model is very crude, the agreement between these two numbers is still considered satisfactory.

In Refs. 3 and 4 for cylinders Z1 and Z2 (with masses of 93.5 and 92.7 g, with $d = 2.31$ and 2.26 cm, with $l = 1.93$ and 2.02 cm, respectively), experimental cumulative numbers of d-d reactions of $(6.26 \pm 1.06) \times 10^4$ and $(5.3 \pm 0.6) \times 10^4$ were obtained, respectively. The ratio between these numbers results in AH1/Z1 = (1.30 ± 0.25) and AH1/Z2 = (1.57 ± 0.19). These ratios must be compared with predictions of Eq. (18), resulting in 1.08 and 1.11, respectively. Again, this is a reasonable agreement, especially if it is taken into account that the experimental cumulative numbers for Z1 and Z2 correspond to an integration time of $t \approx 2t_L$ only. The measurements with slab AH1 during ECS3 also give the possibility of a sensitive estimate of the d-d molecular fusion rate $\Lambda_{d\text{-}d}$ as determined by Eq. (2): After a long loading time (several units of t_L), a rather small reaction rate is predicted by the plasma model. This is in agreement with the experiment. For $\Delta t = 480$ to 760, the ACRD in CHR3 is -1.4 ± 1.0 h^{-1}. Taking into account the detector efficiency and the shadow effect, this results in a d-d reaction rate of $\dot{N}^{d\text{-}d} = 0 \pm 33\ s^{-1}$. For CHR2, in analogy to this, the resulting d-d reaction rate is within the limits $\dot{N}^{d\text{-}d} = 0 \pm 20\ s^{-1}$. This gives the possibility of determining the upper limits of the d-d molecular fusion rate in the massive, fully loaded cathode using Eq. (2). The upper limit of $\Lambda_{d\text{-}d}$, resulting only from the 1σ error bars, is therefore

$$\Lambda_{d\text{-}d} < 1.1 \times 10^{-26}\ s^{-1} \ .$$

The resulting upper limits of specific reaction rates are given by $< 3.20 \times 10^{-5}\ g^{-1} \cdot s^{-1}$ or $< 3.26 \times 10^{-4}\ cm^{-3} \cdot s^{-1}$ of the palladium cathode. These numbers are not in contradiction but are even lower than the upper limits given in several experiments searching for d-d fusion in condensed matter.[10,11] As discussed in Ref. 1, these upper limits also set strong limits for the possible influence of cosmic rays on the production of neutrons in the fully loaded palladium metal. From the fact that no stationary d-d fusion rate was observed from a fully loaded massive slab for 280 h, it can be concluded that it might lead to physically false conclusions if positive effects observed temporarily are interpreted in the framework of a D_2 molecular picture. Therefore, any physical interpretation of positive effects observed in terms of Eq. (2) is omitted.

VII. CONCLUSION

The experiment with a compact palladium slab over >900 h using a sensitive fast neutron spectrometer shows very weak but definite signals of neutrons that most likely result from d-d reactions. However, these effects become observable experimentally only after >90 h of loading because of the large loading time constant t_L of the thick slab used in this experiment.

After ~700 h of loading for a long observation time, the sample shows a negligible d-d reaction effect, even less than the shadow effect caused by the cell itself.

This allows an upper limit to be set for the D_2 molecular fusion rate $\Lambda_{d\text{-}d}$ per deuteron pair per second in a fully loaded sample under stationary conditions, which is given by $\Lambda_{d\text{-}d} < 10^{-26}\ s^{-1}$. This is in agreement with numerous experiments that look for d-d neutrons from metallic samples loaded with deuterium, e.g., in Refs. 10 and 11. As mentioned in Ref. 1, this also provides an upper limit for cosmic muon-induced d-d reactions under stationary conditions: Every cosmic muon stopped in the palladium sample definitely produces fewer than four d-d neutrons. (Even two neutrons per stopped muon would still have been detected.)

In between, slab AH1 during ECS2 shows definite increasing effects up to the end of this cycle, which are continued during the first half of ECS3 that follows.

The maximum effect counting rate in CHR3 for single measurements is of the order of $20 \pm 5\ h^{-1}$, corresponding to a d-d reaction rate of $660 \pm 165\ h^{-1}$. From our measurements it cannot be concluded whether or not count rates would be higher for shorter intervals. However, if averaging takes place for larger intervals, the maximum count rates decrease, as shown in Figs. 2 and 6. This is because the effects observed fluctuate strongly. After averaging over broad time intervals, however, they show a typical time structure comparable to the predictions of a crude plasmalike model. This model predicts a maximum d-d reaction rate under nonequilibrium conditions of charging the cathode with deuterons near $t \simeq t_L$.

Adjusting the model curve to the absolute height of observed average effects, one gets the plasma fusion rate

$$\lambda_{d\text{-}d}^{Pl} = (1.0 \pm 0.15) \times 10^{-44}\ s^{-1} \ ,$$

which is in agreement with the results obtained for cylindrical samples Z1 and Z2 (Refs. 3 and 4).

This plasma fusion rate $\lambda_{d\text{-}d}^{Pl}$ must be directly compared with calculations of the reactivity $\langle v_d \sigma_{d\text{-}d} \rangle$ in a plasma (see, e.g., recent papers by Hora et al.,[12] Scalia,[13] and Rice et al.[14]). In doing this, however, it must be taken into account that in the solid state, only a part of the deuterons are freely movable and that not only a physically founded nonequlibrium velocity distribution but also the effects of electron screening and fluctuation enhancement must be taken into account. Corresponding analyses are needed to get a deeper insight into the physical nature of the plasma fusion rate $\lambda_{d\text{-}d}^{Pl}$ obtained here, which might show quite specific and complicated features.

REFERENCES

1. M. BITTNER, A. MEISTER, D. OHMS, E. PAFFRATH, D. RAHNER, R. SCHWIERZ, D. SEELIGER, K. WIESENER, and P. WÜSTNER, "Method for Investigation of Fusion Reactions in Condensed Matter," *Fusion Technol.*, **18**, 120 (1990).

2. D. SEELIGER and A. MEISTER, "A Simple Plasma Model for the Description of d-d Fusion in Condensed Matter," *Fusion Technol.*, **19**, 2114 (1991).

3. M. BITTNER et al., "Evidence for the Production of d-d Fusion Neutrons During Electrolytic Infusion of Deuterons into a Palladium Cylinder," *Fusion Technol.*, **19**, 2119 (1991).

4. M. BITTNER et al., "Emission of DD-Fusion Neutrons from a Massive Palladium Cylinder During Electrolytic Infusion of Deuterons into the Metal," *Isotopenpraxis*, **6** (1991).

5. D. SEELIGER et al., "Search for DD-Fusion Neutrons During Heavy Water Electrolysis," *Electrochim. Acta*, **34**, 7, 991 (1989).

6. H. O. MENLOVE et al., "Measurement of Neutron Emission from Ti and Pd in Pressurized D_2 Gas and D_2O Electrolysis

Cells," LA-UR:89-1974, Los Alamos National Laboratory (July 27, 1989).

7. A. TAKAHASHI et al., "Emission of 2.45 MeV and Higher Energy Neutrons from D_2O-Pd Cell Under Biased-Pulse Electrolysis," *J. Nucl. Sci. Technol.*, **27**, 7, 663 (1990).

8. G. AHLEFELD and J. VÖLKL, "Hydrogen in Metals I," *Topics in Applied Physics*, Vol. 28, p. 322, Springer-Verlag, Berlin (1979).

9. S. E. JONES et al., "Observation of Cold Nuclear Fusion in Condensed Matter," *Nature*, **338**, 737 (1989).

10. H. FRIEDMANN et al., "Search for Cold Fusion," *Kerntechnik*, **55**, 3, 161 (1990).

11. H. WIESMANN, "Examination of Cathodically Charged Palladium Electrodes for Excess Heat, Neutron Emission, or Tritium Production," *Fusion Technol.*, **17**, 350 (1990).

12. H. HORA et al., "Plasma and Surface Tension Model for Explaining the Surface Effect of Tritium Generation at Cold Fusion," *Nuovo Cimento*, **12D**, 393 (1990).

13. A. SCALIA, "The Nuclear Fusion Rate for Reactions $^2H(d,n)$ and $^2H(d,p)$," *Nuovo Cimento*, **101A**, 795 (1989); see also *Nuovo Cimento*, **102A**, 953 (1989).

14. R. A. RICE et al., "The Role of Velocity Distribution in Cold Deuterium-Deuterium Fusion," *Fusion Technol.*, **18**, 147 (1990).